Continuous-Microflow Synthesis and Morphological Characterization of Multiscale Composite Materials Based on Polymer Microparticles and Inorganic Nanoparticles

Isabelle Kraus[1]*, Shuning Li[2], Andrea Knauer[2], Marc Schmutz[3], Jacques Faerber[1], Christophe A. Serra[4] and Michael Köhler[2]

[1]*Institut de Physique et Chimie des Matériaux de Strasbourg (IPCMS), Université de Strasbourg, CNRS UMR 7504, 23 rue du Læss, BP 43, F-67034 Strasbourg 2, France*
[2]*Department of Physical Chemistry and Microreaction Technology, Institute of Physics, Technical University of Ilmenau, Weimarer Straße 32 PF 100565, D-98684, Ilmenau, Germany*
[3]*Institut Charles Sadron (ICS), CNRS UPR 22, Université de Strasbourg, 23 rue Læss, F-67083, Strasbourg, France*
[4]*Groupe d'Intensification et d'Intégration des Procédés Polymères (G2IP), Institut de Chimie et Procédés pour l'Énergie, l'Environnement et la Santé (ICPEES)-UMR 7515 CNRS, École Européenne de Chimie, Polymères et Matériaux (ECPM), Université de Strasbourg, 25 rue Becquerel, F-67087, Strasbourg, France*

Received: 28 October 2013; accepted: 19 January 2014

This paper presents a new route to the synthesis of uniform and size-controlled inorganic/organic composite microparticles by means of microreaction technology. Au-nanoparticles in the range of 3 to 14 nm are synthesized by reduction of tetrachloroauric acid, while ZnO-nanoparticles (200–2000 nm) are synthesized in a continuous-flow two-step process using microtube arrangements for microsegmented flow. Both inorganic nanoparticles have a well-controlled size and narrow size distribution. Upon surface modification, the nanoparticles are then mixed on one hand with an acrylate-based monomer and, on the other hand, with an aqueous solution of acrylamide. Both solutions were then emulsified into uniform core-shell droplets by means of a capillary-based microfluidic device. Droplet's shell was hardened through UV-induced polymerization, whereas the core led to a hydrogel upon thermal-induced polymerization. Core-shell polymer microparticles (200–300 μm) with inorganic nanoparticles selectively incorporated into the core and the shell are thus obtained as proven by extensive morphological characterizations using electronic and optical microscopies.

Keywords: inorganic nanoparticle, polymer microparticle, composite, microreaction technology, microfluidics, microscopy

1. Introduction

Despite all progress in molecular synthesis, there is an urgent challenge for new routes to prepare nanomaterials. Well-defined composition, properties, and geometries above the level of atomic arrangement are demanded for new functional materials and nanoparticle architectures. Multiscale particles are one promising approach for meeting these requirements. The preparation of such multiscale particles, including nanosized components with high monodispersity, requires strictly controlled conditions for interfaces formation and chemical reaction. Therefore, microreaction technology is well suited [1]. Thus, microreaction technology was applied for the preparation of dielectric [2, 3], semiconductor [4, 5], and metallic nanoparticles [6–8]. The introduction of continuous-microflow processes for these syntheses leads to the constant production of materials at low scale and to an improvement of nanoparticles quality [9, 10]. Thus, the use of the specific advantages of microdroplet generation, microsegmented flow, and flow-focusing allows the generation of monodispersed metal and metal oxide nanoparticles, of monodisperse polymer particles as well as the incorporation of inorganic nanoparticles in polymer composite microparticles [11–13].

Colloidal solutions of nanoparticles with diameters between about 2 and 100 nm can be obtained by different preparation methods. Microfluidics-based methods can be used for a significant improvement of the particle size homogeneity. Besides the pure gold nanoparticles, binary and multishell nanoparticles come into the focus of interest [14–16]. Particles of this type can also be prepared by wet chemical methods. However, the use of microfluid segments leads to a strong process improvement. Flow segmentation causes a complete suppression of fluidic dispersion which is normally observed in standard microfluidic systems due to the low Reynolds numbers. In addition, the use of a carrier liquid having a low contact angle with the hydrophobic wall material leads to a strong reduction of the interaction between the reaction mixture and the wall. Thus, the wall-induced nucleation and particle deposition on the inner wall surfaces are drastically reduced. The principle of microsegmented flow ensures an ideal slug flow and an extremely narrow residence time distribution [17]. The flow-induced segment-internal convection causes fast mixing inside nanoliter fluid segments [18]. The technique can be applied for the two-step synthesis of Au/Ag core/shell nanoparticles with high homogeneity [19] and for the hydrothermal continuous-flow synthesis of ZnO micro- and nanoparticles [20]. On the other hand, the application of microfluidic devices with coaxial arrangements of fluid channels and flow-focusing allows the preparation of different kinds of polymer particles with very high reproducibility [21, 22].

For the synthesis of well-designed composite particles and multiscale materials with high homogeneity of components in size and shape, different microfluidic synthesis methods should be used. The application of microsegmented flow for generating inorganic nanoparticles in the nanometer and lower micrometer range and the application of droplet-based microfluidic systems for the synthesis of polymer microparticles in the middle and upper micrometer range represent two complementary technological strategies. They should be applicable for making homogeneous multiscale materials. The characterization of such obtained multiscale materials can be achieved using optical and electronic microscopies [23, 24].

Here, the continuous-flow microfluidic synthesis of polymer-based multiscale core-shell composite microparticles incorporating plasmonic metal nanoparticles and fluorescent ZnO nanoparticles is reported.

* Author for correspondence: isabelle.kraus@ipcms.unistra.fr

DOI: 10.1556/JFC-D-13-00029

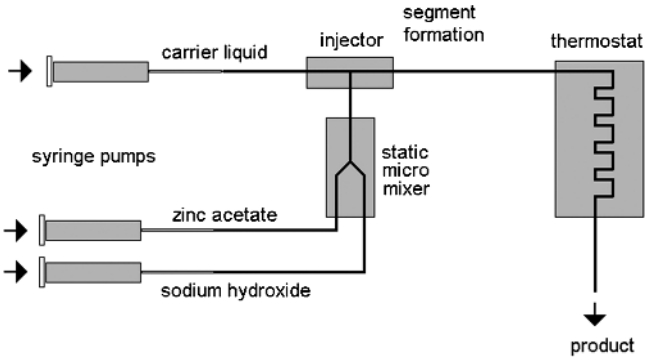

Figure 1. Experimental arrangement for generation of ZnO nanoparticles in microfluid segments

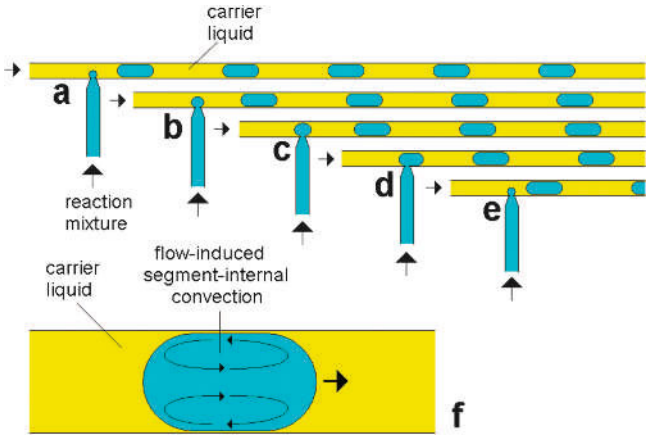

Figure 2. Formation of microfluid segments (a–e) and appearance of a segment-internal convection supporting a fast heat transfer between channel walls and reaction fluid element (f)

2. Materials and methods

2.1. Microfluidic Systems. Two different microfluidic systems are used: 1) a microtube-based segmented-flow arrangement for the synthesis of the ZnO nanoparticles; 2) a capillary-based device for the emulsification of the monomer phase and the downstream hardening of droplets into core-shell composite microparticles.

2.2. Microtube-Based Segmented-Flow System. This system (Figure 1) is composed of three PC-controlled syringe pumps (Nemesys, Cetoni) delivering the fluids at a constant and pulse-free flow rate, a static micromixer (StatMix6, IPHT), a 1/16 in. injector (P-632 Tee Assy, Besta-Technik GmbH) for the generation of the fluid segments and PTFE knotmixers (200 cm length, 0.5 mm ID) placed inside a temperature-controlled block (80 °C) where the hydrothermal synthesis of ZnO nanoparticles is performed. The micromixer is built up in form of a three-chip sandwich system (22 mm × 14 mm) consisting of two glass chips and one silicon chip. The silicon chip in the crystallographic orientation (110) is wet etched anisotropically in order to get microchannels with perpendicular orientated side walls. The etch depth in the silicon chip amounts to 0.5 mm corresponding to the complete thickness of the silicon wafer. The lateral channel width is about 0.2 mm. The glass chips are wet etched isotropically in order to get half round channels. The channel depth and width are about 0.2 mm and 0.4 mm, respectively. The microchannels generated by anodic bonding of the micropatterned substrates are forming a static micromixer of the split-and-recombine type with eight microchannel units for separation, reshaping, and reunification of liquid flow [25, 26].

The microfluid segments are generated at room temperature after the static micromixer. PTFE tube material is used for conducting the reaction mixture from the static micromixer to the injector. The injector and the fluid interfaces are also made of PTFE. This material ensures a good wetting for the carrier liquid and low wetting for the reaction mixture. The microfluid segments are always generated by injecting the reactive solution into a stream of tetradecane (Fisher Scientific) acting as an inert and water-immiscible carrier as well as a separation liquid.

The formation of microfluid segments (droplet-like small portions of reaction mixture) occurs very reproducible. The principle is shown in Figure 2. During the injection, a droplet of the reaction mixture is formed at the injector nozzle (a), it grows up to filling the most part of the channel cross-section (b and c) and forms a cylindrical segment or slug (d) which is finally released after reaching a certain size (e). The microsegmented-flow ensures a common experience of all reaction volume elements during the downstream heating process. The ultimate narrow residence time distribution leads to a uniform temperature history for all fluid segments. At the applied high flow rates, the flow-induced segment-internal convection leads to an efficient enhancement of convective heat exchange between the environment and the reaction mixture (Figure 2f). So, a microflow-based homogenization of liquid heating is realized for initiating ZnO particle formation during the hydrothermal synthesis.

2.3. Capillary-Based Device. The capillary-based device used to synthesize core-shell microparticles (Figure 3) is composed of two co-axial capillaries inserted along the main axis of 1/16 in. T-junctions (PEEK, Upchurch) and syringe pumps (PHD 2000, Harvard Apparatus). The inner capillary (ID 20 × OD 90 µm) has hydrophilic inner walls (fused silica capillary, Polymicro) while the middle capillary (ID 150 × OD 360 µm) has hydrophobic inner walls (PEEK, Upchurch). The middle phase, which ultimately leads to the microparticle's shell, is delivered through the second inlet of the first T-junction and exits at the tip of the inner capillary (Figure 3). Finally, the continuous phase is injected via the second inlet of the second T-junction. Both capillary's tips exit from the second T-junction in the centerline of a 500-µm ID PTFE tubing (Bioblock). Upon formation of the double droplet, the shell is hardened by photopolymerization under UV-irradiation directly in the outlet PTFE tubing, while the core is thermally polymerized at 90 °C offline in a beaker.

2.4. Materials

2.4.1. Inorganic Nanoparticles. For the preparation of hydrophilic Au nanoparticles, 1.0 mM of tetrachloroauric acid (Roth) is reduced first by 30 mM sodium borohydride or sodium citrate (Sigma) in aqueous solution at room temperature in a round bottom flask. For the preparation of hydrophobic Au nanoparticles, the reduction is performed in a water/toluene two-phase system in presence of surfactant (hexadecylamine, Merck).

ZnO particles are obtained using the microfluidic device described in Section 2.1.1 (Figure 1) from the hydrothermal treatment at high pH of a stream, resulting from the mixing of two aqueous solutions containing zinc acetate ($Zn(O_2CCH_3)_2$; Acros)

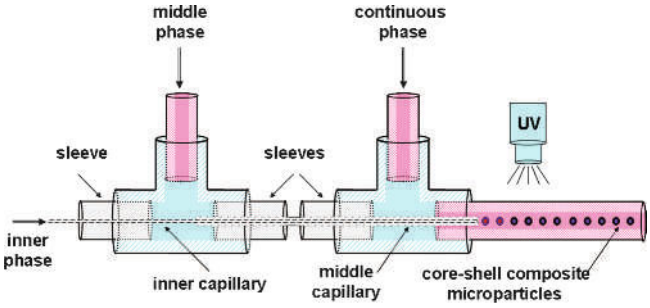

Figure 3. Schematic drawing of the capillary-based system for the production of core-shell composite microparticles

Table 1. Composition of the stream mixture for ZnO microparticles

Particle type	Zn(O2CCH3)2	NaOH	Thermostat temperature	Solvent
Compact (Figure 5a)	20 mM	0.20 M	100 °C	35 % water + 65 % ethanol
Polyhedral-like (Figure 5b)	20 mM+tetramethylammonium hydroxide in presence of polyethylene glycol	none	80 °C	DMSO
Flower-like (Figure 5c)	50 mM	1.00 M	150 °C	water
Star-like (Figure 5d)	100 mM	1.75 M	150 °C	water

Table 2. Composition of the middle phase mixture

	Au composite	ZnO composite
Monomer	72 wt.%	95 wt.%
Photoinitiator	3 wt.%	4 wt.%
Nano-ZnO powder	–	1 wt.%
Nano-Au/toluene solution	25 wt.%	–

and sodium hydroxide (Merck), respectively. Various concentrations and reactions temperatures were investigated in order to generate different types of particles as indicated in Table 1. The resultant nano- and microparticles are dried to form a fine powder which is used as obtained.

2.4.2. Polymer Core-Shell Microparticles. The polymer core-shell microparticles are obtained using the device described in Section 2.1.2 (Figure 3). The continuous phase is composed of a solution of 1.5 wt.% methyl cellulose (Alfa Aesar) in distilled water. The middle phase is composed of a mixture of an acrylate-based monomer (tri(propylene glycol) diacrylate, TPGDA; Aldrich), a photoinitiator (1-hydroxycyclohexyl phenyl ketone, HCPK; Aldrich) and nano-Au/toluene solution or nano-ZnO powder according to the weight percentages given in Table 2.

The inner phase is composed of a hydrophilic monomer (acrylamide, AA, Aldrich), a crosslinker (N,N′-methylene-bisacrylamide, Aldrich), a photoiniator (ammonium persulfate, APS, Aldrich), distilled water and nano-Au/water solution or nano-ZnO powder according to the weight percentages given in Table 3.

2.4.3. Characterization. Au-nanoparticles are characterized by dynamic light scattering (DLS) and optical microscopy under dark field illumination. ZnO nanoparticles are characterized by scanning electron microscope (SEM) (JSM 6380, JEOL). Composite microparticles are observed by optical microscopy under dark field illumination, and by fluorescence with an exciting source at 366 nm and an emission at 420 nm. They are further

Table 3. Composition of the inner phase mixture

	Au-ZnO/core-shell composite	ZnO-Au/core-shell composite
Monomer	8 wt.%	5 wt.%
Crosslinker	0.1 wt.%	0.1 wt.%
Photoiniator	0.1 wt.%	0.1 wt.%
Distilled water	66.8 wt.%	94.3 wt.%
Nano-ZnO powder	–	0.5 wt.%
Nano-Au/water solution	25 wt.%	–

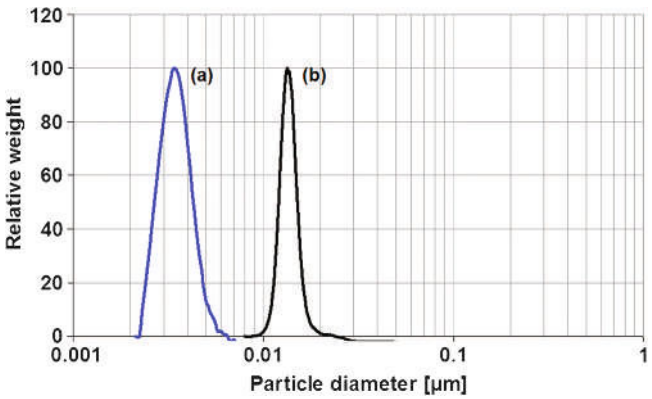

Figure 4. Au nanoparticles size distribution. (a) Au NPs reduced by sodium borohydride (diameter: 3.4 nm); (b) Au NPs reduced by sodium citrate (diameter: 13.3 nm)

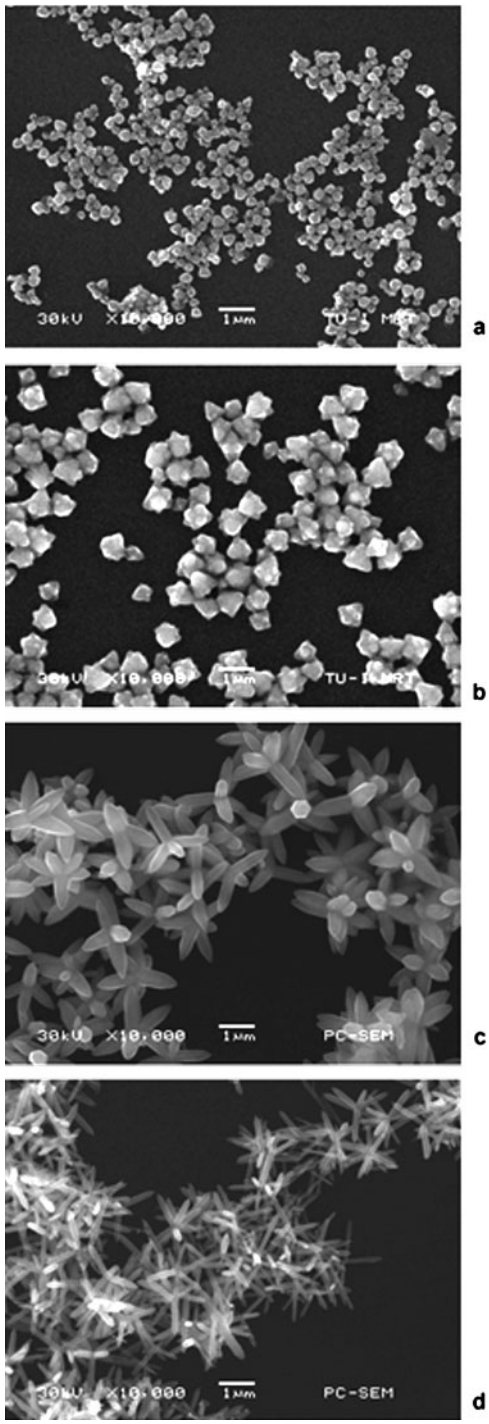

Figure 5. Different types of ZnO particles obtained by continuous-microflow synthesis in microfluid segments under hydrothermal conditions but different concentrations demonstrating the obtained high particle homogeneity for all particle types: a) compact particles, b) polyhedral-like particles, c) flower-like particles, d) star-like particles

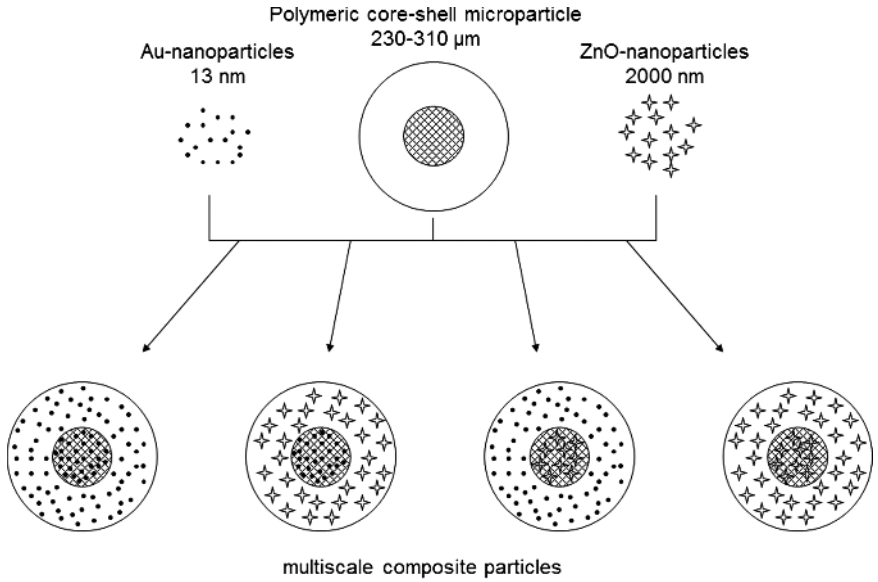

Figure 6. Schematic drawing of the concept of multiscale composite particles (not at scale)

Table 4. Flow rate of the different phases and diameter of synthesized core-shell microparticles

	Outer phase (mL/min)	Middle phase (mL/min)	Inner phase (mL/min)	Particle diameter (µm)
Figure 7A/Au–Au	0.02	0.0025	0.001	310
Figure 7B/Au–ZnO	0.06	0.0025	0.001	250
Figure 7C/ZnO–Au	0.05	0.0025	0.001	230
Figure 7D/ZnO–ZnO	0.05	0.0025	0.001	240

characterized by SEM to measure their outer diameter (imaging software Hiris; R&D Vision) and to observe their surface [23]. Microparticles are also cut in pieces with a razor blade to investigate their internal structure and composition. SEM secondary electron images and back-scattered electrons images in chemical Z-contrast (COMPO) are then recorded (JEOL 6700 F), and energy dispersive X-rays spectrometry (EDXS) (Thermo-Noran Vantage) is performed to identify the chemical composition. Ultramicrotomy slices are performed on embedded microparticles in EPON resin (ultramicrotom, UCT; Leica). Semi-thin sections of 300 nm (nominal thickness) are prepared for optical and florescence microscopies [24]. Thin sections of 50 nm (nominal thickness) are used for transmission electron microscopy (TEM) observations (TECNAI Sphera G2, FEI).

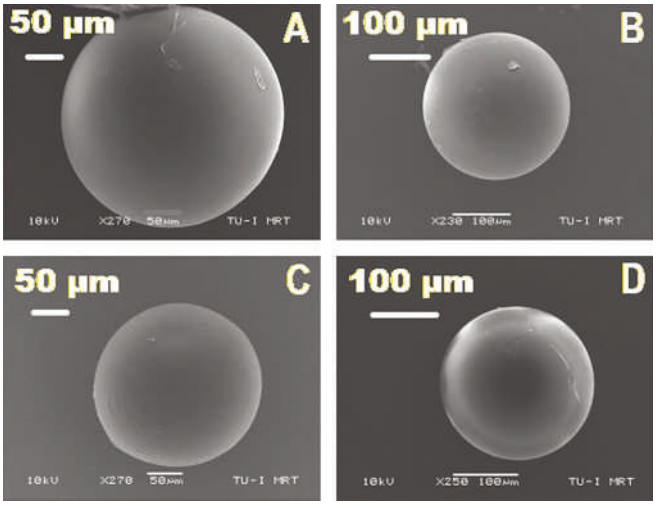

Figure 7. SEM micrographs of composite poly(AA)-poly(TPGDA)/ core-shell microparticles with: A) Au-Au/core-shell nanoparticles, B) Au-ZnO/core-shell nanoparticles, C) ZnO-Au/core-shell nanoparticles, D) ZnO-ZnO/core-shell nanoparticles

3. Results and Discussion

3.1. Nanoparticles Synthesis. Gold nanoparticles are obtained by the reduction of tetrachloroauric acid with sodium borohydride in aqueous solution or with sodium citrate. The stronger sodium borohydride reducing agent causes a fast nucleation, which results into a high number of small particles. Citric acid is a weaker reducing agent, hence the particle formation is marked by a lower nucleation rate and by a nucleation/precipitation mechanism [27]. This results into a lower particle density but a higher volume of single particles. Upon mixing, the appearance of an intensive red color indicates the fast formation of nano-Au. This color is due to the plasmon resonance absorption of the metal nanoparticles. DLS experiment performed on the colloidal solution shows that the average diameter of the nanoparticles is about 13 nm or 3.4 nm, depending on the reducing agent (Figure 4).

Zinc oxide nanoparticles are obtained from the hydrothermal synthesis at high pH in aqueous solution, using the microfluidic device described in Section 2.1.1. The zinc acetate solution and

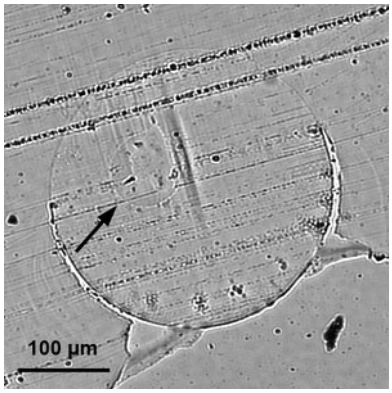

Figure 8. Optical image of a thin-section of a composite ZnO/ZnO core-shell microparticle embedded in resin. The black arrow indicates the slightly off-centered poly(AA) core

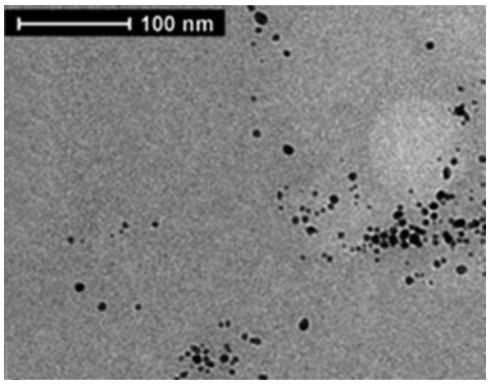

Figure 9. TEM micrograph of an ultramicrotomy slice showing the Au nanoparticles (black spots) embedded in a poly(TPGDA) microparticle

the sodium hydroxide solution are mixed continuously at room temperature by conducting both liquids through the static micromixer (Figure 1). No precipitation takes place in this phase due to the formation of zinc hydroxide complexes. This reaction mixture is then transferred into the injector in order to generate a segmented flow. The segments are conducted into the thermostat in order to thermally initiate the ZnO formation. The appearance of ZnO particles with sizes between submicron and a few microns becomes visible by the arising opacity of the reaction mixture. The nucleation and the growth of ZnO nano- and microparticles are strongly affected by the pH (NaOH content), by the solvent nature, and by the concentration of available Zn^{2+} ions. Thus, different types of particles can be generated when reactant concentrations and reaction conditions are varied (Figure 5, Table 1). Compact, polyhedral, flower-like, or star-like particles are generated in dependence of concentration of NaOH and zinc acetate. In contrast to most batch synthesis, a high homogeneity in shape and size of ZnO particles is found for small compact as well as for larger flower-like or star-like particles during the preparation under a continuous-microflow regime using the microfluid segment technique. The time needed for heat transfer and/or mixing in classical synthesis experiments causes a certain spatial distribution of concentrations as well as reaction conditions and is responsible for a larger distribution of particle sizes and shapes in many cases. On the other hand, the fast mixing and fast heat transfer achieved under microfluidic conditions reduce these inhomogeneities [20, 28, 29]. As a result, a higher quality of particles is obtained.

3.2. Synthesis of Multiscale Composite Core-Shell Microparticles. The concept of multiscale composite particles consists of polymer microparticles composed of two sub-domains (shell and core) selectively embedding inorganic nanoparticles (Au or ZnO) whose size is by several orders of magnitude smaller than the polymer microparticle diameter (Figure 6). To achieve this multiscale morphology, the inorganic nanoparticles must be introduced into the monomer phase before droplets formation.

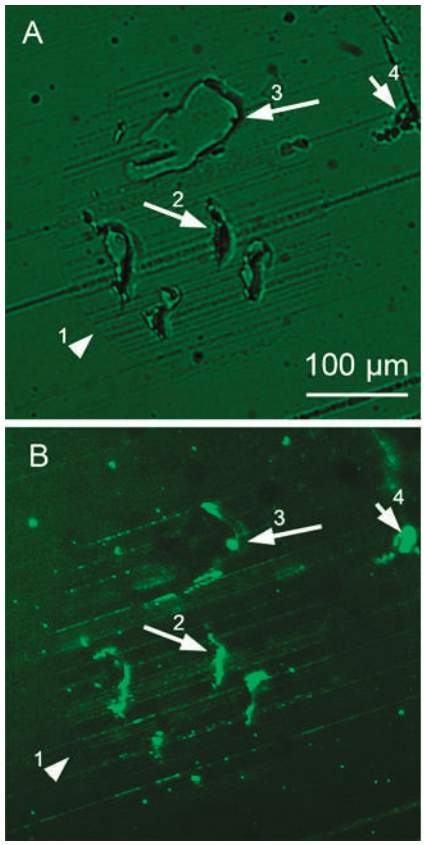

Figure 11. Thin sections (300 nm) of an embedded core-shell microparticle observed under fluorescence microscopy. Rips obtained during the cutting process can be seen with ZnO nanoparticles located on their edges, facing the front of the cutting direction. The section is seen under optical bright field microscopy (A) and fluorescence microscopy (B). The shell outer limit of the microparticle is clearly seen. Arrow 1 points to the interface between the polymer matrix and the resin. Arrows 2 and 3 point to the ZnO nanoparticles confirmed by their fluorescence in panel B. Arrow 4 shows an extracted ZnO-nanoparticle.

Four different poly(AA)-poly(TPGDA)/core-shell microparticles having selective distribution of Au- or ZnO-particles are prepared by a co-axial capillaries microfluidic device. About 2000 nm flower-like ZnO-particles (Figure 5c) are used. The core-shell particles mean diameter varies from 230 to 310 µm, depending on the outer phase flow rate (Table 4). In droplet microfluidics, higher shear rate induced by higher outer phase flow rate is known to produce smaller microparticles [30, 31]. SEM micrographs (Figure 7) show that the composite microparticles have smooth surface and that no aggregation of inorganic nanoparticles is visible on the surface.

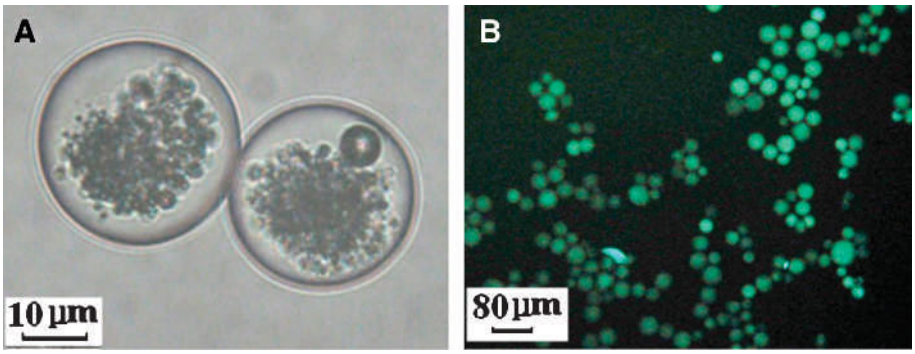

Figure 10. Optical images of Poly(TPGDA) microparticles with ZnO nanoparticles seen by A) dark field; B) fluorescence

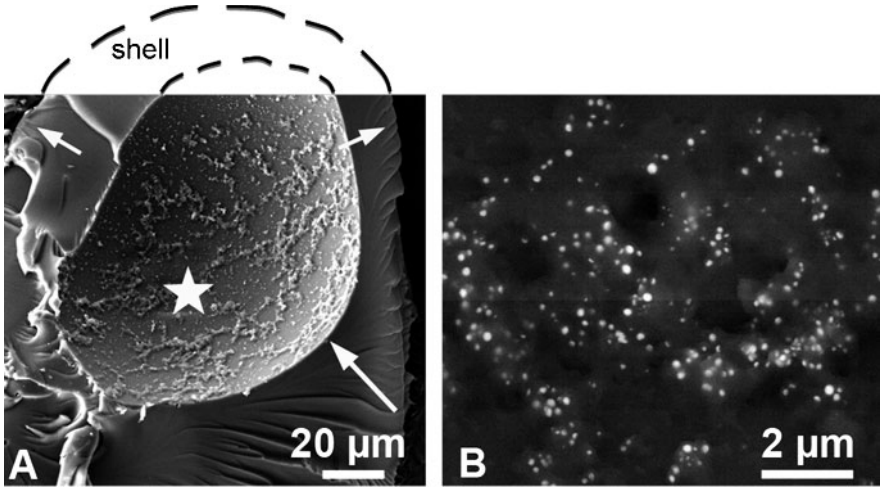

Figure 12. Cut ZnO/Au core-shell microparticle. A) Due to the preparation process, the hydrogel core is fully retracted, leaving the core-shell interface visible (long white arrow). This interface is covered by aggregates, formed of ZnO-nanoparticles and dried poly(acrylamide). The short white arrow points to the outer surface of the shell. The white star locates the region investigated in panel B. B) "COMPO-image" of the core-shell interface. The white dots indicate a chemical difference of composition which is identified as Zn by EDX spectroscopy

To further characterize the ultrastructure of the core-shell microparticles, we performed thin sectioning of the beads to study their inner morphology by optical microscopy and fluorescent microscopy. Figure 8 shows a 300-nm-thick section of a ZnO/ZnO core-shell particle. The core can be seen within the shell, clearly off-centered (black arrow). It is the case for some studied samples. We performed serial sections on a bead. The one presented in Figure 8 is a sagittal plane so that the diameters seen are inferior to the real diameters of the core and shell. Dark spots are ZnO particles, confirmed by fluorescence microscopy.

The successful embedding of Au-nanoparticles into a polymer microparticle has already been demonstrated in a previous paper [1]. The microparticle has a smooth surface, and no inorganic nanoparticles aggregation is to be seen. This suggests that the nanoparticles are trapped within the polymer matrix only. The random dispersion of Au nanoparticles inside the polymer microparticle is revealed by TEM analysis of a nano-Au/Poly(TPGDA) microparticle ultramicrotomy slice (Figure 9). One can clearly see that 13 nm Au nanoparticles are present in the matrix.

The question now arises for the successful embedding of ZnO nanoparticles within the desired sub-domain. For a plain microparticle (one domain), optical images performed (Figure 10A) show that the nanoparticles are concentrated in the central part of the polymer bead. Fluorescence microscopy (Figure 10B) reveals the strong fluorescent properties of these particles.

To confirm the presence of ZnO nanoparticles in our core-shell microparticles, we observed the thin sections under fluorescence microscopy (Figure 11). In some cases, large rips can be observed in sections. They are cutting artefacts. The difference in stiffness of the polymer matrix versus the ZnO nanoparticles leads to a disruption during the cutting process. It is stopped when the constraints are released either by the cutting of the ZnO nanoparticle or by its extraction from the polymer matrix. Indeed, ZnO nanoparticles can be observed attached on the edges of the rips (Figure 11B). The observed size of the fluorescent spots does correspond to the one observed for non-incorporated ZnO nanoparticles. From time to time, some ZnO nanoparticles are observed outside the bead area. They have been sectioned or full size particles have been extracted from the polymer matrix during the cutting process (Figure 11, arrow 4). The localization of the rips, homogeneously distributed all over the sectioned bead area and the absence of rips beginning at the resin/polymer interface, indicates that the ZnO particles have been embedded homogeneously within the polymer matrix and that they are not confined at the interface.

In some rare cases, we observed heavy off-centered core-shell particles. In that case, we noticed when cutting the microparticle in pieces that the core is missing, leaving a deposition of ZnO nanoparticle aggregates on the inner surface of the shell (i.e. the expected core-shell interface). This is clearly visible in the SEM image of Figure 12, for which Zn element has been identified by means of a back-scattered electrons image in chemical Z-contrast (COMPO image) and EDX spectroscopy. This confirms that one can selectively incorporate nanoparticles in a multi-domain microparticle.

4. Conclusion

Multiscale composite materials were prepared in continuous-microflow systems from inorganic nanoparticles and core-shell polymer microparticles. Au- or ZnO-nanoparticles were synthesized in a microchannel-based reactor offering an improved control over their size and size distribution. Poly(AA)-poly(TPGDA)/ core-shell polymer microparticles were synthesized from the emulsification of the monomer mixtures into double droplets thanks to a co-axial capillary-based device. Once hardened through thermal- or UV-induced polymerization, the droplets formed inorganic-filled polymer microparticles in the size range of few hundreds of micrometers with an extremely narrow size distribution. Following this procedure, several uniform and size-controlled inorganic/organic composite microparticles were prepared: four different poly(AA)-poly(TPGDA)/core-shell microparticles having nano-Au or nano-ZnO in the shell and/or in the core. Microreaction technology was proven as an efficient technology for the synthesis of multiscale composite materials whose specific properties resulting from the different orders in size may find applications in, e.g., sensorics or biomedical.

Acknowledgments. The authors are grateful to the PHC PROCOPE, through project no. 17900PG, for having supported the student exchange expenditures in-between the research groups. CS is grateful to the French Ministry of Higher Education and Research for having funded this work through the grant ANR no. NT05-1_45715. Z. Chang is acknowledged for the help in the experiments as well as Danièle Spehner (IGBMC, Illkirch) regarding the embedding procedure.

References

1. Chang, Z.; Serra, C. A.; Bouquey, M.; Kraus, I.; Li, S.; Köhler, J. M. *Nanotechnology,* **2010**, *21*, 015605.

2. Cottam, B. F.; Krishnadasan, S.; DeMello, A. J.; DeMello, J. C.; Shaffer, M. S. P. *Lab. Chip*. **2007** 167–169
3. Donnet, M.; Jongen, N.; Lemaitre, J.; Bowen, P. *J. Mat. Sci. Lett*. **2000**, *19*, 749–750.
4. Guillemet-Fritsch, S.; Aoun-Habbache, S.; Sarrias, J.; Rousset, A.; Jongen, N.; Donnet, M.; Bowen, P.; Lemaitre J. *Solid State Ionics* **2004**, *171*, 135–140.
5. Winterton, J. D.; Myers, D. R.; Lippmann, J. M.; Pisano, A. P.; Doyle, F. M. *J. Nanopart. Res*. **2008**, *10*, 893–905.
6. Wagner, J.; Köhler, J. M. *Nano Lett*. **2005**, *5*, 685–691
7. Weng, C.-H.; Huang, C.-C.; Yeh, C.-S.; Lei, H-Y.; Lee, G.-B. *J. Micromech. Microengn*. **2008**, *18*, 035019.
8. Cabeza, V. S.; Kuhn, S.; Kulkarni, A. A.; Jensen, K. F. *Langmuir* **2012**, *28*, 7007–7013.
9. Knauer, A.; Thete, A.; Li, S.; Romanus, H.; Csaki, A.; Fritzsche, W.; Köhler, J. M. *Chem. Eng. J*. **2011**, *116*, 1164–1169.
10. Knauer, A.; Csaki, A.; Möller, F.; Hühn, C.; Fritzsche, W.; Köhler, J. M. *J. Phys. Chem*. **2012**, *116*, 9251–9258.
11. Gross, G. A.; Hamann, C.; Günther, M.; Köhler, J. M. *Chem. Eng. Technol*. **2007**, *30*, 341–346.
12. Köhler, J. M.; Kraus, I.; Faerber, J.; Serra, Ch. *J. Mat. Sci*. **2013**, *48*, 2158–2166.
13. Köhler, J. M.; März, A.; Popp, J.; Knauer, A.; Kraus, I.; Faerber, J.; Serra, C. *Anal. Chem*. **2013**, *85*, 313–318.
14. Link, S.; Wang, Z. L.; El-Sayed, M. A. *J. Phys. Chem*. **1999**, *B103*, 3529–3533.
15. Moskovits, M.; Smova-Sloufova, I; Vlcková, B. *J. Chem. Phys*. **2002**, *116*, 10435–10446.
16. Rodriguez-González, B.; Burrows, A.; Wanatabe, M.; Kiely, C. J.; Liz Marzán, L. M. *J. Mat. Chem*. **2005**, *15*, 1755–1759.
17. Teh, S.-Y.; Lin, R.; Hung, L.-H.; Lee, A. P. *Lab Chip* **2008**, *8*, 198–220.
18. Aoki, N.; Mae, K. *Chem. Eng. J*. **2006**, *118*, 189–197.
19. Köhler, J. M.; Held, M.; Hübner, U.; Wagner, J. *Chem. Eng. Tech*. **2007**, *30*, 347–354.
20. Li, S.; Günther, P. M.; Köhler, J. M. *J. Chem. Eng*. **2009**, *42*, 338–345.
21. Serra, C.; Chang, Z. *Chem. Eng. Tech*. **2008**, *31*, 1099–1115.
22. Serra, C.; Berton, N.; Bouquey, M.; Prat, L.; Hadziioannou, G. *Langmuir* **2007**, *23*, 7745–7750.
23. Sawyer, L. C.; Grubb, D. T. *Polymer microscopy;* Chapman and Hall, London, UK, 1996.
24. Jönsson, J.-E.; Karlsson, O. J.; Hassender, H.; Törnell, B. *Eur. Poly. J*. **2007**, *43*, 1322–1332.
25. Kirner, T.; Albert, J.; Günther, M.; Mayer, G.; Reinhäckel, K.; Köhler, J. M. *Chem. Eng. J*. **2004**, *101*, 65–74.
26. Köhler, J. M.; Wagner, J.; Albert, J. *J. Mat. Chem*. **2005**, *15*, 1924–1930.
27. Polte, J.; Ahner, T.; Delissen, F.; et al. *J. Am. Chem. Soc*. **2010**, *132*, 1296–1301
28. Li, S.; Meierott, S.; Köhler, J. M. *Chem. Eng. J*. **2010**, *165*, 958–965.
29. Köhler, J. M.; Li, S.; Knauer, A. *Chem. Eng. Technol*. **2013**, *36*, 887–899.
30. Chang, Z.; Serra, C.; Bouquey, M.; Prat, L.; Hadziioannou, G. *Lab. Chip*. **2009**, *9*, 3007–3011.
31. Yobas, L.; Martens, S.; Ong, W. L.; Ranganathan, N. *Lab. Chip*. **2006**, *6*, 1073–1079.